



# Continuous-wave operation of vertically emitting ring interband cascade lasers at room temperature

Cite as: Appl. Phys. Lett. **116**, 131101 (2020); <https://doi.org/10.1063/1.5139649>

Submitted: 21 November 2019 . Accepted: 14 March 2020 . Published Online: 30 March 2020

Hedwig Knötig , Borislav Hinkov , Robert Weih, Sven Höfling, Johannes Koeth, and Gottfried Strasser 



View Online



Export Citation



CrossMark

## ARTICLES YOU MAY BE INTERESTED IN

[High power edge-cum-surface emitting terahertz laser arrays phased locked by vacuum guided plasmon waves](#)

Applied Physics Letters **116**, 131103 (2020); <https://doi.org/10.1063/1.5142860>

[Spin-transport in superconductors](#)

Applied Physics Letters **116**, 130501 (2020); <https://doi.org/10.1063/1.5138905>

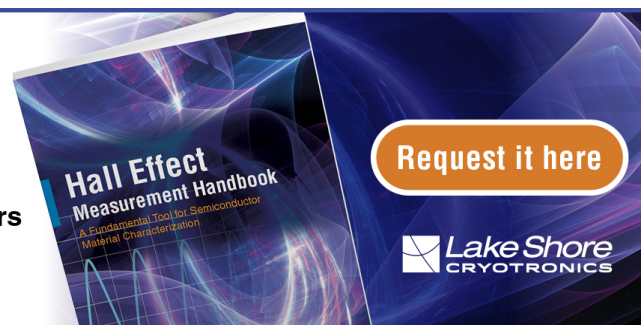
[A wire waveguide channel for terabit-per-second links](#)

Applied Physics Letters **116**, 131102 (2020); <https://doi.org/10.1063/1.5143699>

## Hall Effect Measurement Handbook

**A comprehensive resource for researchers**

Explore theory, methods, sources of errors, and ways to minimize the effects of errors



Request it here

 Lake Shore  
CRYOTRONICS



# Continuous-wave operation of vertically emitting ring interband cascade lasers at room temperature

Cite as: Appl. Phys. Lett. **116**, 131101 (2020); doi: [10.1063/1.5139649](https://doi.org/10.1063/1.5139649)

Submitted: 21 November 2019 · Accepted: 14 March 2020 ·

Published Online: 30 March 2020






View Online



Export Citation



CrossMark

Hedwig Knötig,<sup>1,a)</sup>  Borislav Hinkov,<sup>1</sup>  Robert Weih,<sup>2</sup> Sven Höfling,<sup>3,4</sup> Johannes Koeth,<sup>2</sup> and Gottfried Strasser<sup>1,5</sup> 

## AFFILIATIONS

<sup>1</sup>Institute of Solid State Electronics, TU Wien, 1040 Vienna, Austria

<sup>2</sup>nanoplus Nanosystems and Technologies GmbH, 97218 Gerbrunn, Germany

<sup>3</sup>Technische Physik, Physikalisches Institut, University Würzburg, 97074 Würzburg, Germany

<sup>4</sup>SUPA, School of Physics and Astronomy, University of St Andrews, St Andrews, KY16 9SS, United Kingdom

<sup>5</sup>Center for Micro- and Nanostructures, TU Wien, 1040 Vienna, Austria

<sup>a)</sup> Authors to whom correspondence should be addressed: [hedwig.knoetig@tuwien.ac.at](mailto:hedwig.knoetig@tuwien.ac.at)

## ABSTRACT

We present vertical light emission in continuous-wave mode from an interband cascade laser (ICL) at a record temperature of up to 38 °C. These results pave the way toward a more efficient and compact integration of this technology in mobile spectroscopic applications. Our approach employs ring cavity ICLs that are mounted epi-side down for efficient heat extraction from the devices. The vertical single-mode emission relies on a metallized second-order distributed-feedback grating designed for an emission wavelength of 3.8 μm. A single lateral mode operation is favored by a narrow waveguide width of 4 μm. Optical output powers of more than 6 mW were measured at 20 °C for rings with a diameter of ~800 μm. At this temperature, the threshold current-density amounted to 0.60 kA/cm<sup>2</sup> and the device showed continuous current and temperature tuning rates of 0.06 nm/mA and 0.37 nm/K, respectively.

© 2020 Author(s). All article content, except where otherwise noted, is licensed under a Creative Commons Attribution (CC BY) license (<http://creativecommons.org/licenses/by/4.0/>). <https://doi.org/10.1063/1.5139649>

A large variety of gaseous chemicals display their fundamental molecular absorption features (attributed to vibrations and rotations) in the mid-infrared spectral region, spanning the wavelength range from 2.5 μm to 14 μm.<sup>1</sup> Hence, this region is of particular interest for gas spectroscopy. Many sensitive detection schemes require laser sources offering continuous-wave (cw) operation at room temperature and designable and tunable emission wavelengths.<sup>2</sup>

Since their first proposal in 1995,<sup>3</sup> interband cascade lasers (ICLs) have advanced to reliable sources covering wavelengths from 2.8 μm to 5.6 μm in cw operation at room temperature in the GaSb material system.<sup>4,5</sup> ICLs based on InAs have recently been shown to extend this range to wavelengths beyond 6 μm.<sup>6,7</sup> ICLs typically show low power consumption and low lasing threshold current<sup>8</sup> in comparison to quantum cascade lasers (QCLs),<sup>9,10</sup> which are, up to now, the dominant mid-IR laser sources. Thus, they are especially attractive for mobile, miniaturized, and battery-powered sensing applications. While edge-emitting ICLs based on GaSb are operating in cw mode at room temperature,<sup>2</sup> vertical light emission has so far been limited to pulsed operation<sup>11,12</sup> or to lower temperatures.<sup>13</sup> A vertical-cavity

surface-emitting laser (VCSEL) based on type-II quantum wells (QWs) in a single-stage active region was shown to operate in cw mode up to -7 °C at 4 μm,<sup>13</sup> while devices relying on type-I QWs achieved cw operating temperatures of up to 5 °C at 3 μm.<sup>14</sup> These compact devices rely on the epitaxial growth of high-quality Bragg mirrors above and below the gain material, thus automatically ensuring operation in a single longitudinal mode.<sup>15,16</sup> In our work, we are using ICLs fabricated into ring-shaped cavities. In contrast to VCSELs, where the maximum output power is limited due to their relatively small gain volume, the output power of ring ICLs can be scaled by adjusting the width and diameter of the waveguide.<sup>12</sup> In addition, surface emitters do not rely on a cleaved facet for light emission, as opposed to edge-emitting devices. No additional phase difference is introduced by the position of the cleave edge with regard to the grating as for ridge devices, making the wavelength selection more accurate. Furthermore, surface emission permits the integration of multiple devices in a two-dimensional array.<sup>17</sup> In the case of substrate-emission, other optical elements like polarizers<sup>18</sup> or meta-material lenses<sup>19</sup> can be directly integrated on the substrate-side of the device,

further increasing the level of monolithic integration and broadening possible applications.

With the aim of achieving vertical light emission in cw mode at room temperature, in this study, we design and realize a ring device based on a second-order distributed-feedback (DFB) grating. This geometry has a twofold application. First, it allows the wavelength selection and second, the outcoupling of the light from a ring cavity, in this case through the substrate. In previous studies, epi-side up mounting in combination with a multiple mm-wide hole in the heat sink was used to facilitate the collection of light, limiting the devices to pulsed operation due to poor thermal dissipation.<sup>12</sup> In this work, we report on epi-side down mounted ring ICLs allowing cw operation at temperatures of up to 38 °C. In addition, the width of the waveguide is reduced to 4  $\mu\text{m}$  compared to 10  $\mu\text{m}$ <sup>12</sup> for the first generation of devices, to suppress lasing of higher order lateral modes.<sup>20</sup> To compensate for the resulting reduction in optical output power due to the smaller gain area, an outer ring diameter of  $\sim 799 \mu\text{m}$  was chosen to obtain an active volume corresponding to a device with a ridge waveguide of length 2.5 mm.

The active region of the ICL comprises six stages with a design-wavelength of 3.8  $\mu\text{m}$ , relying on a W-type QW design (two coupled InAs-QWs separated by a GaInSb barrier: 2.50 nm AlSb/1.90 nm InAs/2.40 nm Ga(0.68)In(0.32)Sb/1.47 nm InAs/1.00 nm AlSb). Two 200 nm-thick GaSb separate-confinement layers (SCLs) sandwich the active region. High modal gain is provided in this way, confining the mode in the center of the waveguide due to a higher refractive index of the SCLs. The active core region is further sandwiched between InAs/AlSb superlattice claddings of lower refractive index. The epitaxial layers were grown by molecular beam epitaxy on a single-side polished n-GaSb (100) substrate.

Detailed information on the device fabrication can be found in Ref. 12. In the following, we point out the major differences and structure improvements compared to the previously published ring ICLs.<sup>12</sup> The waveguide and grating etch is performed in a Cl/Ar-chemistry using an inductively coupled plasma (ICP) reactive ion etching (RIE) process as opposed to the previously used SiCl<sub>4</sub>/Ar-process. This leads

to more vertical slightly positively sloped sidewalls as compared to the observed negative slope using the former process. The waveguide etch is stopped in the GaSb SCL below the active region in a total etch depth of 3  $\mu\text{m}$ . We use a grating etch depth of 910 nm, a grating period of  $\Lambda_g = 1.141 \mu\text{m}$ , and an effective grating duty cycle of  $\sigma \sim 60\%$ . After both these etch steps, a phosphoric acid-based wet etch is performed in order to smoothen the sidewalls and reduce surface-roughness induced absorption losses. A thinner electrical passivation layer of 250 nm Si<sub>3</sub>N<sub>4</sub> is deposited and selectively removed from a wider contact window (3.9  $\mu\text{m}$ ) on top of the ring. The devices are metallized via sputtering of 30 nm/650 nm Ti/Au layers. To facilitate single device cleaving, the GaSb substrate is thinned down to a thickness of 170  $\mu\text{m}$  and consecutively polished using a 0.1  $\mu\text{m}$ -diamond lapping film to reduce scattering of the emitted light at the substrate surface. Ti/Au bottom contacts (10 nm/200 nm) were sputtered on the backside, leaving an uncovered circular area with a diameter of 1.2 mm for substrate emission. The scanning electron microscopy image of a final device is shown in Fig. 1(a). The top right inset shows a focused ion beam (FIB) cut through the grating, revealing its periodic structure. The grooves are not fully filled with gold, which comes from the directional sputtering beam. However, this issue is solved during the following soldering step of the epi-side down process. When using a soft solder like indium, they get filled up during the soldering process in an epi-side down configuration of the device to the heatsink, granting a good thermal extraction of heat from the device. Epi-side down mounting allows us to have a superior heat extraction compared to standard epi-up soldering. First, individual rings are cleaved from the whole chip. Then, each ring is picked up via a vacuum tip and placed on a copper plate with a thin layer of indium solder. A hotplate is used to heat up indium to 150 °C, melting it in order to bond it to the sputtered gold of the top contact of the ring ICL.

To measure the emitted optical output power, a power meter (Thorlabs S401C) is placed directly in front of the substrate side of the laser. All measurements are performed with the ring ICLs running in cw operation. Figure 1(b) depicts the light-current-voltage characteristics of the device at submount temperatures ranging from 14 °C to

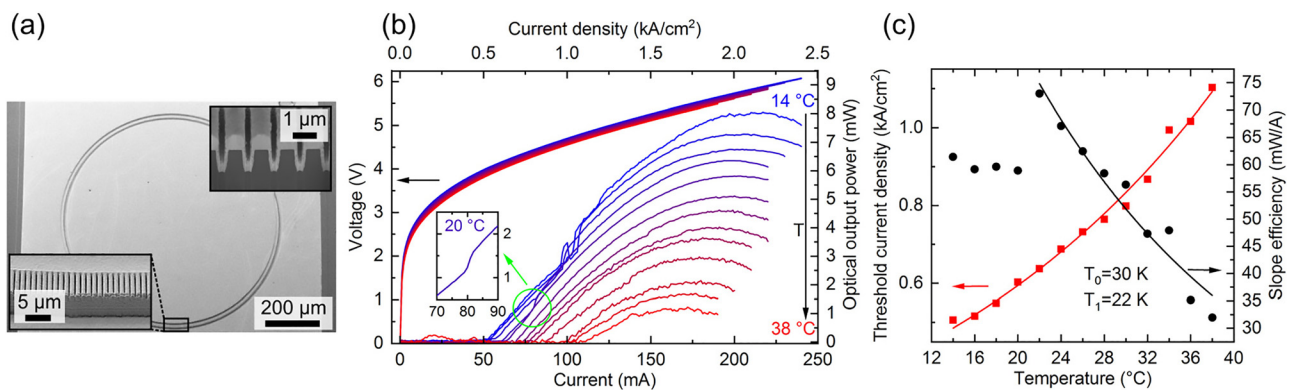


**FIG. 1.** (a) Scanning electron micrograph of a fabricated ring interband cascade laser. A close-up of the metallized second-order distributed feedback grating is shown in the bottom-left inset. The top right inset shows an image of a FIB cut in the middle of the waveguide through the grating structure. (b) Light-current-voltage characteristics of the ring ICL in cw operation at different submount temperatures with steps of 2 °C (14 °C–38 °C). The light at an emission wavelength of  $\sim 3.8 \mu\text{m}$  is measured using a power meter. The inset shows a jump in optical output power at a temperature of 20 °C. (c) Threshold current densities (red squares) and differential slope efficiencies (black circles) measured at different heatsink temperatures (14 °C–38 °C) and the corresponding fits (red and black lines) are shown. The characteristic temperatures of  $T_0 = 30 \text{ K}$  and  $T_1 = 22 \text{ K}$  are subsequently extracted.

38 °C in steps of 2 °C. At the lowest measured temperature of 14 °C, an optical output power of 8 mW was measured. The maximum optical output power at 20 °C amounts to ~6.4 mW. At this temperature, a threshold current (density) of 60 mA (0.60 kA/cm<sup>2</sup>) is extracted for the reported geometry. At 20 °C, two regimes can be identified in the optical output power, with a jump in the optical measurement occurring at  $I = 81$  mA [see the inset in Fig. 1(b)], which is further investigated within spectral characterization. The characteristic temperatures  $T_0$  and  $T_1$  are extracted from exponential fits to the measurement data of the threshold current density  $J_{th}$  and the slope efficiency  $\eta$ , respectively, as functions of the submount temperature  $T$ . This is shown in Fig. 1(c). The exponential fits  $J_{th} = J_0 \cdot \exp(T/T_0)$  and  $\eta = \eta_0 \cdot \exp(-T/T_1)$  yield characteristic temperatures of  $T_0 = 30$  K and  $T_1 = 22$  K, respectively. State-of-the-art ridge ICLs typically show values between 45 and 60 K for  $T_0$  in pulsed operation.<sup>2</sup> In comparison, the value obtained from cw measurements is lower, due to the higher thermal load of the device under operation. At a temperature of 20 °C, slope efficiencies of 59 mW/A and 70 mW/A are measured before and after the jump in the optical output power, indicating two different operation regimes. Therefore, this point and all lower temperatures are omitted in the fit. At a heatsink temperature of 22 °C, the differential slope efficiency of 73 mW/A equates to an external differential quantum efficiency of ~23% ( $\eta_{ext} = \frac{\text{number of emitted photons per unit time}}{\text{number of electrons passing through the structure per unit time}}$ ). Although measured

in cw mode, the slope efficiency is higher than the reported value for a 15-stage interband cascade VCSEL<sup>11</sup> in pulsed operation (~52 mW/A at 20 °C). This is an indication of better performance of our approach in this regard because, in general, when going from pulsed to cw operation, the inevitable increased thermal load of the device will worsen its performance. Even when assuming optimal heat extraction, this will at best result in the same slope efficiency as in pulsed operation.

For spectral characterization, the light is collimated with a BF<sub>2</sub> ( $f = 50$  mm) lens and directed toward a Bruker Equinox 55 Fourier transform infrared (FTIR) spectrometer, where it is measured using a wide-range deuterated triglycine sulfate (DTGS) detector. For these measurements, the FTIR is operated in the standard rapid-scan mode. Figure 2(a) shows emission spectra of the lasing ring device driven at a current of  $I = 140$  mA. Single-mode emission of the ring ICL is observed over the entire range of 15 °C to 35 °C around a wavelength of ~3.84  $\mu\text{m}$  with a spectral spread of 7 nm. The shift in the laser emission wavelength is due to a temperature driven change in the refractive index, related to a linear temperature tuning coefficient of  $\Delta\lambda/\Delta T = 0.37$  nm/K ( $\Delta\nu/\Delta T = -0.25$  cm<sup>-1</sup>/K). More vital for spectroscopic applications are the tuning characteristics of the laser with the driving current, as it is a faster way of scanning through different wavelengths than using the thermal effect. Emission spectra recorded at a submount temperature of 20 °C starting at the threshold current

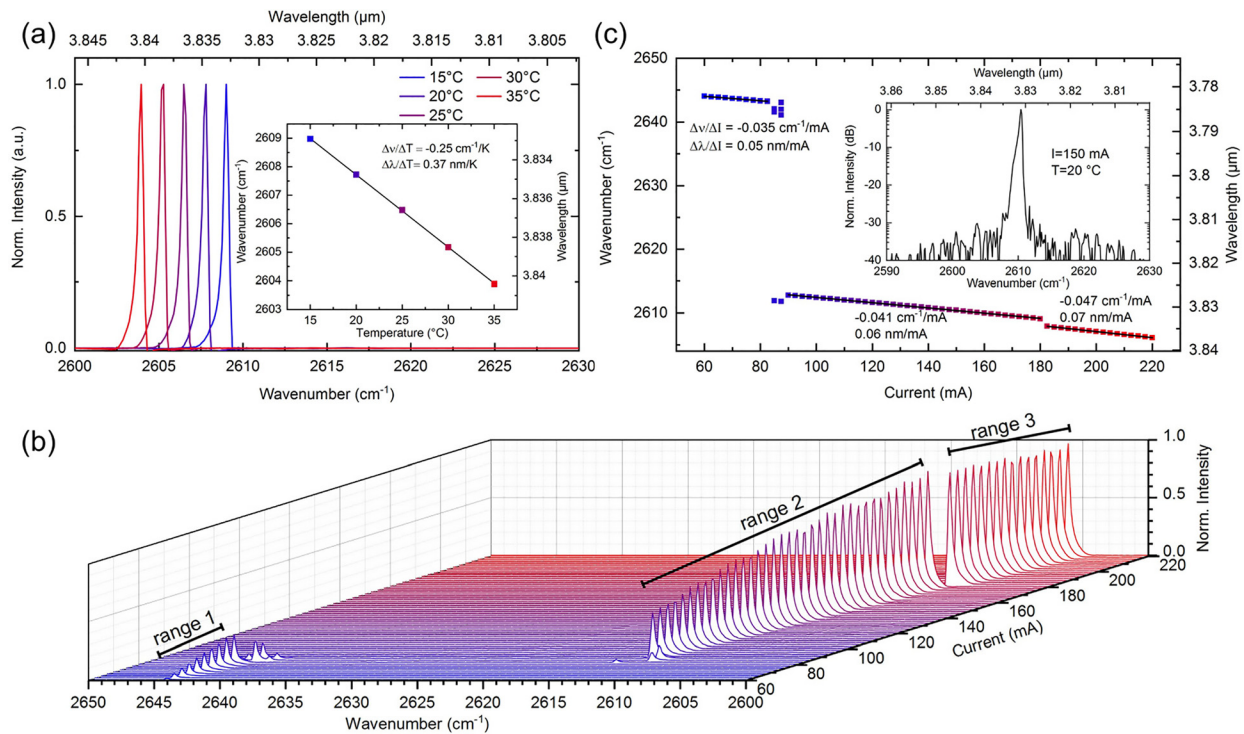


**FIG. 2.** (a) Emission spectra of the ring ICL obtained at different heatsink temperatures and a fixed drive current of  $I = 140$  mA. The inset shows the change in the emission wavelength with temperature, corresponding to an extracted linear temperature tuning coefficient of  $\Delta\lambda/\Delta T = 0.37$  nm/K ( $\Delta\nu/\Delta T = -0.25$  cm<sup>-1</sup>/K). (b) Spectral output of the ring device at a heatsink temperature of 20 °C and at different drive currents ranging from 60 mA to 220 mA. Three different ranges can be identified separated by two jumps in the wavelength occurring at ~81 mA and 180 mA. The main portion of the spectrum (range 2) still shows continuous tuning, spanning 3.7 cm<sup>-1</sup> (4.4 nm) from 90 mA to 180 mA. (c) Current tuning characteristics of the ring ICL at a heatsink temperature of 20 °C as well as the corresponding linear current tuning coefficients. The emission spectrum of the ring device ( $I = 150$  mA and  $T = 20$  °C) is depicted on a semi-logarithmic scale showing a side mode suppression ratio >25 dB.

( $I_{th} = 60$  mA) and extending beyond the thermal roll-over to a drive current of 220 mA in steps of 1.5 mA are shown in Fig. 2(b). The laser displays single-mode emission over the entire range, except for a narrow transition region around  $\sim 81$  mA, where a mode jump in the emission wavelength occurs from  $\nu = 2643$   $\text{cm}^{-1}$  to  $2613$   $\text{cm}^{-1}$ . This mode jump coincides with the jump in optical output power seen in Fig. 1(b), which can, therefore, be traced back to a shift in the gain at these different wavelengths. A second jump of the wavelength takes place at 180 mA from  $\nu = 2609$   $\text{cm}^{-1}$  to  $2608$   $\text{cm}^{-1}$ ; however, this does not lead to a change in the output power, because the wavelengths are close to each other, and thus, the gain is comparable. We attribute the jumps in optical output power at lower temperatures ( $14^\circ\text{C}$ – $18^\circ\text{C}$ ) around  $\sim 100$  mA shown in Fig. 1(b) to the occurrence of further mode jumps.

Figure 2(c) depicts the wavelength dependence on the driving current at a submount temperature of  $20^\circ\text{C}$ . Three different spectral regions can be identified, showing a slight increase in the linear current tuning coefficient with increasing current, from  $0.05$  nm/mA to  $0.07$  nm/mA ( $\Delta\nu/\Delta I = -0.035$   $\text{cm}^{-1}/\text{mA} \rightarrow -0.047$   $\text{cm}^{-1}/\text{mA}$ ).

To further investigate the mode hopping and the possible occurrence of higher order lateral modes, optical simulations of the ring waveguide were performed. The waveguide losses retrieved from the imaginary part of the obtained effective refractive index for different waveguide widths are shown in Fig. 3(a). The losses for the higher order radial modes significantly increase with the decreasing waveguide width, as do the losses for the fundamental mode below a waveguide width of  $5$   $\mu\text{m}$ . For a waveguide width of  $4$   $\mu\text{m}$ , the losses for the higher order lateral mode are more than four times as high as those for the fundamental mode. The second-order radial mode for our demonstrated device dimensions is located further toward the outside of the waveguide, as can be seen in the insets of Fig. 3(a). This leads to increased losses due to surface roughness inevitably introduced during the fabrication process at the interface of the different layers on top of the sample surface (SiN, Au, ...). These losses add up and further increase the selectivity in

favor of the fundamental mode. Although a further decrease in the waveguide width would completely eliminate the possibility of an occurring second-order radial mode, it would also lead to higher losses for the fundamental mode, therefore increasing the lasing threshold significantly or even preventing lasing operation at all.

The measured far field of the ring ICL ( $I = 150$  mA and  $200$  mA,  $T = 20^\circ\text{C}$ ) is depicted in Fig. 3(b). As expected from the circular geometry of the device, it is also circularly symmetric. The emission angle of the maximum intensity and the surrounding interference rings is determined by the geometry of the grating and the device.<sup>21</sup> We attribute the inhomogeneities in the intensity distribution to imperfections and defects in the device fabrication, especially the waveguide and grating etching. The far field differs from the almost Gaussian shaped beam profile reported for interband-cascade VCSELs.<sup>11</sup> For the first spectral region at  $20^\circ\text{C}$  below the mode hop (e.g., at  $65$  mA, range 1 in Fig. 2(b)), we observe a second ring of almost equal intensity occurring at around  $10^\circ$  in the far field (not shown), possibly indicating lasing of the ring in the second-order lateral mode or a difference in the coupling of the grating at these operating parameters. Above the first mode hop up until the thermal roll-over of the device, the reported shape of the far field qualitatively remains the same, as can be seen in Fig. 3(b). Far field modifications and how they can be used for specific emission characteristics have already been extensively studied in QCLs<sup>18,19,22</sup> and will be the goal of future studies.

In conclusion, we have demonstrated single-mode emission of ring ICLs running in cw operation up to a temperature of  $38^\circ\text{C}$ . These results are especially compelling as there is a drive for reaching higher operating temperatures with other approaches like VCSELs for vertical emission as well. A VCSEL device, based on two spatially separated active regions containing five ICL stages, was recently demonstrated to work in cw operation up to  $18.5^\circ\text{C}$ .<sup>23</sup> Our devices show output powers of more than  $6$  mW at  $20^\circ\text{C}$  and  $8$  mW at the lowest measured temperature of  $14^\circ\text{C}$ . A metallized second-order DFB

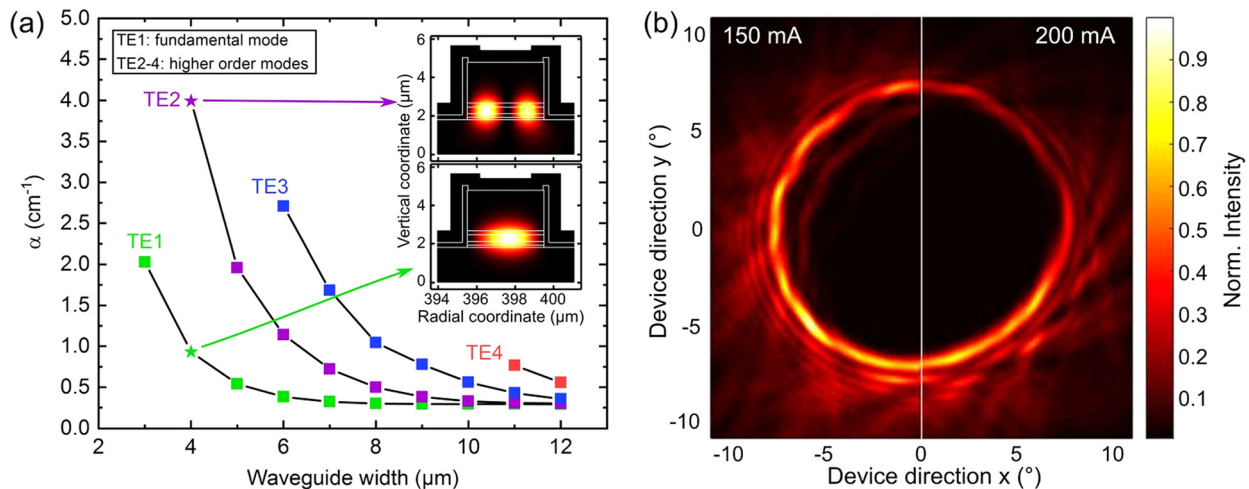


**FIG. 3.** (a) Waveguide losses of the lateral modes obtained from simulations of various waveguide widths. The demonstrated ring ICL supports two radial waveguide modes, which are shown in the insets. The plots show the time-averaged power flow. The losses for the second-order lateral mode are more than four times higher than those for the fundamental mode. (b) Measured substrate emission far fields of the ring ICL at drive currents of 150 mA and 200 mA and a submount temperature of  $20^\circ\text{C}$ . Both the far field measurements were individually normalized.

grating was fabricated to permit both single-mode emission and light extraction through the substrate. The epi-side down mounting ensures sufficient heat removal to permit cw emission at room temperature and above. In addition, this together with the improved fabrication process and design resulted in a reduced threshold current density of  $0.60 \text{ kA/cm}^2$  in cw at  $20^\circ\text{C}$ , compared to the previous ring ICLs, which showed  $0.75 \text{ kA/cm}^2$  in pulsed operation.<sup>12</sup> The smaller waveguide width of  $4 \mu\text{m}$  compared to the previously reported ring ICL devices ( $10 \mu\text{m}$ ) suppressed higher order lateral modes over a large range of operating conditions, facilitating single-mode emission over a larger range of temperatures and currents. A higher output power as well as a lower lasing threshold should be feasible by further improving the fabrication process. This includes employing an improved epi-side down mounting scheme (e.g., using AuSn submounts) and electroplating  $\mu\text{m}$ -thick gold layers on top of the grating, to ensure that the grooves are filled up completely, as well as further reducing the surface roughness of the waveguide. The deposition of an anti-reflection coating on the substrate surface would also be beneficial for light extraction. In addition, we expect that further improvement of the grating design (e.g., the grating duty-cycle<sup>24</sup> and the introduction of  $\pi$ -phase shifts<sup>18</sup>) should enhance the performance of the laser and lead to a low divergence central lobed far field.

The authors are grateful for financial support received under Austrian Research Promotion Agency (FFG) project No. 1516332 (ATMO-SENSE). H.K. would like to thank M. Schinnerl for his help with both the focused ion beam (FIB) cut and the SEM images, which were used for Fig. 1(a), and J. Hillbrand for fruitful discussions and support over the course of this project.

## REFERENCES

- <sup>1</sup>J. Hodgkinson and R. P. Tatam, "Optical gas sensing: A review," *Meas. Sci. Technol.* **24**, 012004 (2013).
- <sup>2</sup>I. Vurgaftman, R. Weih, M. Kamp, J. R. Meyer, C. L. Canedy, C. S. Kim, M. Kim, W. W. Bewley, C. D. Merritt, J. Abell, and S. Höfling, "Interband cascade lasers," *J. Phys. D* **48**, 123001 (2015).
- <sup>3</sup>R. Q. Yang, "Infrared laser based on intersubband transitions in quantum wells," *Superlattices Microstruct.* **17**, 77–83 (1995).
- <sup>4</sup>J. Scheuermann, R. Weih, M. V. Edlinger, L. Nähle, M. Fischer, J. Koeth, M. Kamp, and S. Höfling, "Single-mode interband cascade lasers emitting below  $2.8 \mu\text{m}$ ," *Appl. Phys. Lett.* **106**, 161103 (2015).
- <sup>5</sup>W. W. Bewley, C. L. Canedy, C. S. Kim, M. Kim, C. D. Merritt, J. Abell, I. Vurgaftman, and J. R. Meyer, "Continuous-wave interband cascade lasers operating above room temperature at  $\lambda = 4.7\text{--}5.6 \mu\text{m}$ ," *Opt. Express* **20**, 3235 (2012).
- <sup>6</sup>S. M. S. Rassel, L. Li, Y. Li, R. Q. Yang, J. A. Gupta, X. Wu, and G. C. Aers, "High-temperature and low-threshold interband cascade lasers at wavelengths longer than  $6 \mu\text{m}$ ," *Opt. Eng.* **57**, 011021 (2017).
- <sup>7</sup>R. Q. Yang, L. Li, W. Huang, S. M. S. Rassel, J. A. Gupta, A. Bezinger, X. Wu, S. G. Razavipour, and G. C. Aers, "InAs-Based Interband Cascade Lasers," *IEEE J. Sel. Top. Quantum Electron.* **25**, 1200108 (2019).
- <sup>8</sup>R. Weih, M. Kamp, and S. Höfling, "Interband cascade lasers with room temperature threshold current densities below  $100 \text{ A/cm}^2$ ," *Appl. Phys. Lett.* **102**, 231123 (2013).
- <sup>9</sup>J. Faist, F. Capasso, D. L. Sivco, C. Sirtori, A. L. Hutchinson, and A. Y. Cho, "Quantum cascade laser," *Science* **264**, 553–556 (1994).
- <sup>10</sup>B. Hinkov, A. Bismuto, Y. Bonetti, M. Beck, S. Blaser, and J. Faist, "Singlemode quantum cascade lasers with power dissipation below 1W," *Electron. Lett.* **48**, 646 (2012).
- <sup>11</sup>W. W. Bewley, C. L. Canedy, C. S. Kim, C. D. Merritt, M. V. Warren, I. Vurgaftman, J. R. Meyer, and M. Kim, "Room-temperature mid-infrared interband cascade vertical-cavity surface-emitting lasers," *Appl. Phys. Lett.* **109**, 151108 (2016).
- <sup>12</sup>M. Holzbauer, R. Szedlak, H. Detz, R. Weih, S. Höfling, W. Schrenk, J. Koeth, and G. Strasser, "Substrate-emitting ring interband cascade lasers," *Appl. Phys. Lett.* **111**, 171101 (2017).
- <sup>13</sup>G. K. Veerabathran, S. Sprengel, A. Andrejew, and M.-C. Amann, "Room-temperature vertical-cavity surface-emitting lasers at  $4 \mu\text{m}$  with GaSb-based type-II quantum wells," *Appl. Phys. Lett.* **110**, 071104 (2017).
- <sup>14</sup>A. Andrejew, S. Sprengel, and M.-C. Amann, "GaSb-based vertical-cavity surface-emitting lasers with an emission wavelength at  $3 \mu\text{m}$ ," *Opt. Lett.* **41**, 2799 (2016).
- <sup>15</sup>E. Kapon and A. Sirbu, "Power-efficient answer," *Nat. Photonics* **3**, 27–29 (2009).
- <sup>16</sup>S. Stephan, D. Frederic, and A. Markus-Christian, "Novel InP- and GaSb-based light sources for the near to far infrared," *Semiconductor Sci. and Technol.* **31**(11), 113005 (2016).
- <sup>17</sup>E. Mujagić, C. Schwarzer, Y. Yao, J. Chen, C. Gmachl, and G. Strasser, "Two-dimensional broadband distributed-feedback quantum cascade laser arrays," *Appl. Phys. Lett.* **98**, 141101 (2011).
- <sup>18</sup>C. Schwarzer, R. Szedlak, S. Il Ahn, T. Zederbauer, H. Detz, A. Maxwell Andrews, W. Schrenk, and G. Strasser, "Linearly polarized light from substrate emitting ring cavity quantum cascade lasers," *Appl. Phys. Lett.* **103**, 081101 (2013).
- <sup>19</sup>R. Szedlak, C. Schwarzer, T. Zederbauer, H. Detz, A. Maxwell Andrews, W. Schrenk, and G. Strasser, "On-chip focusing in the mid-infrared: Demonstrated with ring quantum cascade lasers," *Appl. Phys. Lett.* **104**, 151105 (2014).
- <sup>20</sup>W. W. Bewley, C. L. Canedy, C. S. Kim, M. Kim, J. R. Lindle, J. Abell, I. Vurgaftman, and J. R. Meyer, "Ridge-width dependence of midinfrared interband cascade laser characteristics," *Opt. Eng.* **49**, 111116 (2010).
- <sup>21</sup>E. Mujagić, S. Schartner, L. K. Hoffmann, W. Schrenk, M. P. Semtsiv, M. Wienold, W. T. Masselink, and G. Strasser, "Grating-coupled surface emitting quantum cascade ring lasers," *Appl. Phys. Lett.* **93**, 011108 (2008).
- <sup>22</sup>R. Szedlak, M. Holzbauer, D. MacFarland, T. Zederbauer, H. Detz, A. M. Andrews, C. Schwarzer, W. Schrenk, and G. Strasser, "The influence of whispering gallery modes on the far field of ring lasers," *Sci. Rep.* **5**, 16668 (2015).
- <sup>23</sup>V. Jayaraman, S. Segal, F. Towner, K. Lascola, B. Kolasa, D. John, A. Cazabat, and C. Burgner, "Room-Temperature Continuous-Wave Electrically Pumped  $3.3 \mu\text{m}$  Vertical Cavity Laser," in *Conference on Lasers and Electro-Optics Europe & European Quantum Electronics Conference (CLEO/Europe-EQEC)* (IEEE, 2019) pp. 1–1.
- <sup>24</sup>C. Schwarzer, E. Mujagić, S. I. Ahn, A. M. Andrews, W. Schrenk, W. Charles, C. Gmachl, and G. Strasser, "Grating duty-cycle induced enhancement of substrate emission from ring cavity quantum cascade lasers," *Appl. Phys. Lett.* **100**, 191103 (2012).